# **Inorganic Chemistry**

pubs.acs.org/IC Article

# Elucidating the Impact of Rare Earth or Transition Metal Identity on the Physical and Electronic Structural Properties of a Series of Redox-Active Tris(amido) Complexes

Nicholas A. Garcia,<sup>‡</sup> Victoria C. Tafuri,<sup>‡</sup> Rana B. Abdu, and Courtney C. Roberts\*



Cite This: Inorg. Chem. 2024, 63, 15283–15293



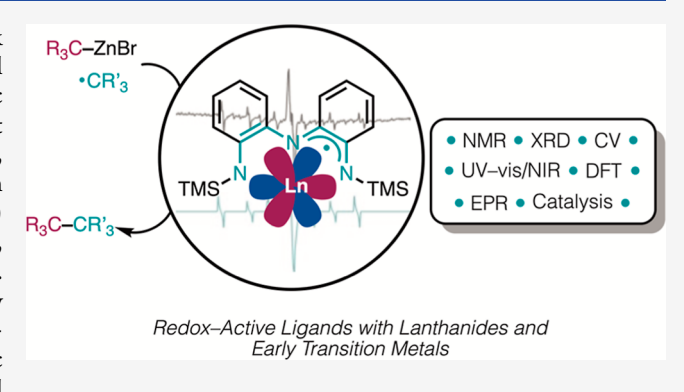
**ACCESS** 

Metrics & More

Article Recommendations

s Supporting Information

ABSTRACT: The use of redox-active ligands with the f-block elements has been employed to promote unique chemical transformations and explore their unique emergent electronic properties for a myriad of applications. In this study, we report eight new tris(amido) metal complexes: 1–Ln (Ln = Tb³+, Dy³+, Ho³+, Er³+, Tm³+, and Yb³+), 1–La, and 1–Ti (an early transition metal analogue). The one-electron oxidation of the tris(amido) ligand was conducted to generate semi-iminato complexes 2–Ln, 2–La, and 2–Ti, and these complexes were studied using EPR. Tris(amido) complexes 1–Ln, 1–La, and 1–Ti were fully characterized using a range of spectroscopic (NMR and UV–vis/NIR) and physical techniques (X–ray diffraction and cyclic voltammetry, with the exception of 1–La). Computational



methods were employed to further elucidate the electronic structures of these complexes. Lastly, complexes 1–Ln, 1–La, and 1–Ti were probed as catalysts for alkyl–alkyl cross-coupling, and the initial rate of the reaction was measured to explore the influence of the metal ion.

# **■ INTRODUCTION**

The chemistry surrounding lanthanide complexes is considerably underdeveloped in comparison to their d-block counterparts. This has led to a recent increase in interest surrounding the unique properties of the complexes such as their larger ionic radii, Lewis acidity, and electronic features. Due to these properties exclusive to the lanthanides, they have been applied in a wide variety of fields including magnetism, catalysis, medical imaging, separations chemistry, and many more. 3–22

The chemistry of the lanthanides is primarily dominated by the Ln3+ oxidation state, as it leads to thermodynamically stable 5d<sup>0</sup> 4f<sup>n</sup> electronic configurations.<sup>23</sup> As a direct result, many Ln3+ complexes normally do not undergo redox processes to perform chemical transformations without the use of harsh oxidizing or reducing agents.<sup>24–33</sup> The exceptions being Ce<sup>4+</sup>, Sm<sup>2+</sup>, Eu<sup>2+</sup>, Tb<sup>4+</sup>, and Yb<sup>2+</sup> due to their propensity to obtain half or fully filled 4f subshells, which are thermodynamically accessible.<sup>23</sup> Evans and co-workers have successfully isolated a series of divalent lanthanide complexes and explored their unique electronic properties.<sup>34</sup> Additionally, exploration of high-valent lanthanide complexes (such as Ce<sup>4+</sup>, Pr<sup>4+</sup>, and Tb<sup>4+</sup>) has been undertaken by the La Pierre, Schelter, and Mazzanti groups, among others.<sup>2,15,35–40</sup> While the renaissance of nonaqueous lanthanide chemistry continues to expand, the use of harsh reductants and oxidants is normally needed to access these redox states in lanthanide complexes.  $^{24-40}$ 

One method to promote redox processes without the use of harsh reagents involves the use of redox-active ligands (RALs) to serve as electron reservoirs. The use of RALs with f element complexes to date remains far rarer than their transition metal counterparts. Limited examples of lanthanide complexes bearing RALs have been used to promote small-molecule activation and redox reactions, cross-coupling, separations chemistry, single molecule magnetism, and luminescent probes in biological systems.<sup>3,41–50</sup> Despite challenges with separations, the greater earth abundance of the lanthanides compared to many second and third row transition metals provides a compelling reason to study their redox chemistry that is enabled by RALs.<sup>51</sup>

Recently, our group reported a series of complexes (1-Sc, 1-Y, 1-Lu, and 1-Zr) bearing a redox-active tris(amido) ligand, previously popularized by Heyduk and co-workers using  $Ta^{5+}$  (Figure 1A). This tris(amido) ligand was

Received: May 8, 2024 Revised: July 15, 2024 Accepted: July 16, 2024 Published: August 5, 2024





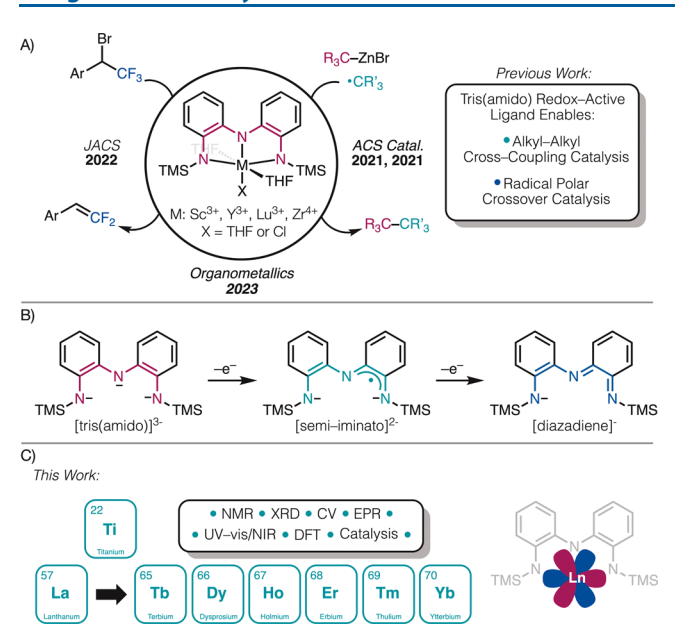


**Figure 1.** (A) Previously reported  $C(sp^3)-C(sp^3)$  cross-coupling and radical-polar crossover catalysis using a tris(amido) RAL. (B) Accessible redox states for the tris(amido) ligand. (C) Incorporation of  $Ti^{4+}$  and a series of  $Ln^{3+}$  ions to complete a series of tris(amido) complexes.

found to undergo two one-electron oxidation events, generating a semi-iminato (ligand radical) and diazadiene (diimine) redox state (Figure 1B). Our group applied these redox properties to promote alkyl–alkyl cross-coupling catalysis, as well as radical–polar crossover catalysis for the synthesis of *gem*-difluoroalkenes. 54–57

With a robust RAL system, we were interested in enabling the RAL chemistry of the lanthanide series. The use of RALs on a series of lanthanide complexes could result in a versatile range of redox potentials that can be altered by the identity of the lanthanide ion. Additionally, the synergistic effects of the RAL and any potential metal-based redox events could result in unique reactivity. We sought to synthesize, isolate, and characterize an isostructural series of lanthanide complexes to determine the impact the lanthanide ion imposes on the redox properties of the tris(amido) ligand. Additionally, we were interested in exploring the emergent electronic properties of the semi-iminato state of the tris(amido) ligand in close proximity to a paramagnetic lanthanide ion. In this study (Figure 1C), we report eight new tris(amido) metal complexes, 1-Ln ( $Ln = Tb^{3+}$ ,  $Dy^{3+}$ ,  $Ho^{3+}$ ,  $Er^{3+}$ ,  $Tm^{3+}$ , and  $Yb^{3+}$ ) and 1-La, along with their spectral and reactivity properties. Due to being the second most abundant transition metal, 1-Ti (the 3d analogue of previously reported 1-Zr) was also synthesized to compare the rare earth series to early transition metals.

# RESULTS AND DISCUSSION

**Synthesis of Tris(amido) Complexes.** Because of the unique properties of the rare earth and group 4 metals, multiple synthetic routes to each desired complex were explored. Complexes 1–Ln (Ln = Tb<sup>3+</sup>, Dy<sup>3+</sup>, Ho<sup>3+</sup>, and Er<sup>3+</sup>) were synthesized either using their respective LnBn<sub>3</sub>(THF)<sub>3</sub> or (Me<sub>3</sub>SiCH<sub>2</sub>)<sub>3</sub>Ln(THF)<sub>2</sub> tris(alkyl) precursors in THF solutions at -78 °C over the course of 18 h through *in situ* deprotonation and metalation pathways (Figure 2). These complexes were isolated as powders in various

Figure 2. Synthesis of tris(amido) complexes.

shades of yellow in moderate yields, ranging from 70-80%. Due to both of the TbBn<sub>3</sub>(THF)<sub>3</sub> and TmBn<sub>3</sub>(THF)<sub>3</sub> complexes never being reported, 1-Tb and 1-Tm were synthesized using the (Me<sub>3</sub>SiCH<sub>2</sub>)<sub>3</sub>Ln(THF)<sub>2</sub> precursors and isolated as yellow powders in 73% (1-Tm) and 70% (1-Tb) yields. Interestingly, the YbBn<sub>3</sub>(THF)<sub>3</sub> complex was not found to be readily isolable. Due to the accessible Yb2+ oxidation state, a Yb2+-Yb3+ ion pair species is readily formed in solution. 58 Use of the (Me<sub>3</sub>SiCH<sub>2</sub>)<sub>3</sub>Yb(THF)<sub>2</sub> precursor resulted in the isolation of 1-Yb as a green powder in a 78% yield. Complexes 1-Ln were readily soluble in ethereal solvents as well as aromatic solvents. Complex 1-Ti was synthesized by adding a solution of a deprotonated tris(amido) ligand dropwise to a suspension of TiCl<sub>4</sub>(THF)<sub>2</sub> in THF at -35 °C in the absence of light. After 4 h, 1−Ti was isolated as a dark green powder in 63% yield. Complex 1-Ti was moderately soluble in hydrocarbon solvents and was soluble in aromatic and ethereal solvents.

Initial attempts to access the La³+ six—coordinate analogue of 1—Ln resulted in the formation of multiple species in THF (Figure 2). Exchanging the solvent from THF to a bidentate donor, such as 1,2—dimethoxyethane (DME), resulted in the successful isolation of the seven-coordinate monomeric complex 1—La in 61% yield. Complex 1—La exhibited limited solubility in aromatic solvents and DME and was insoluble in hydrocarbon solvents. Dissolution of 1—La in other coordinating solvents, such as THF, displaces DME and forms an unsymmetric species in situ (Figure S16), where integrations relative to each other in the ¹H NMR spectrum were consistent with a putative dimeric species with two tris(amido) ligands bound across two La³+ centers.

X-ray Crystallographic Studies. Single-crystal X-ray diffraction studies were conducted on all 1–Ln complexes, 1–La, and 1–Ti. Single crystals of complexes 1–Ln were grown at ambient temperature by layering concentrated THF solutions with pentane. Single crystals of complex 1–La were grown from filtering a saturated, hot DME solution through a Celite pad and allowing it to cool to room temperature slowly. Single crystals of complex 1–Ti were grown from a concentrated solution of THF and stored at –35 °C. The structures display distorted geometries of six-coordinate

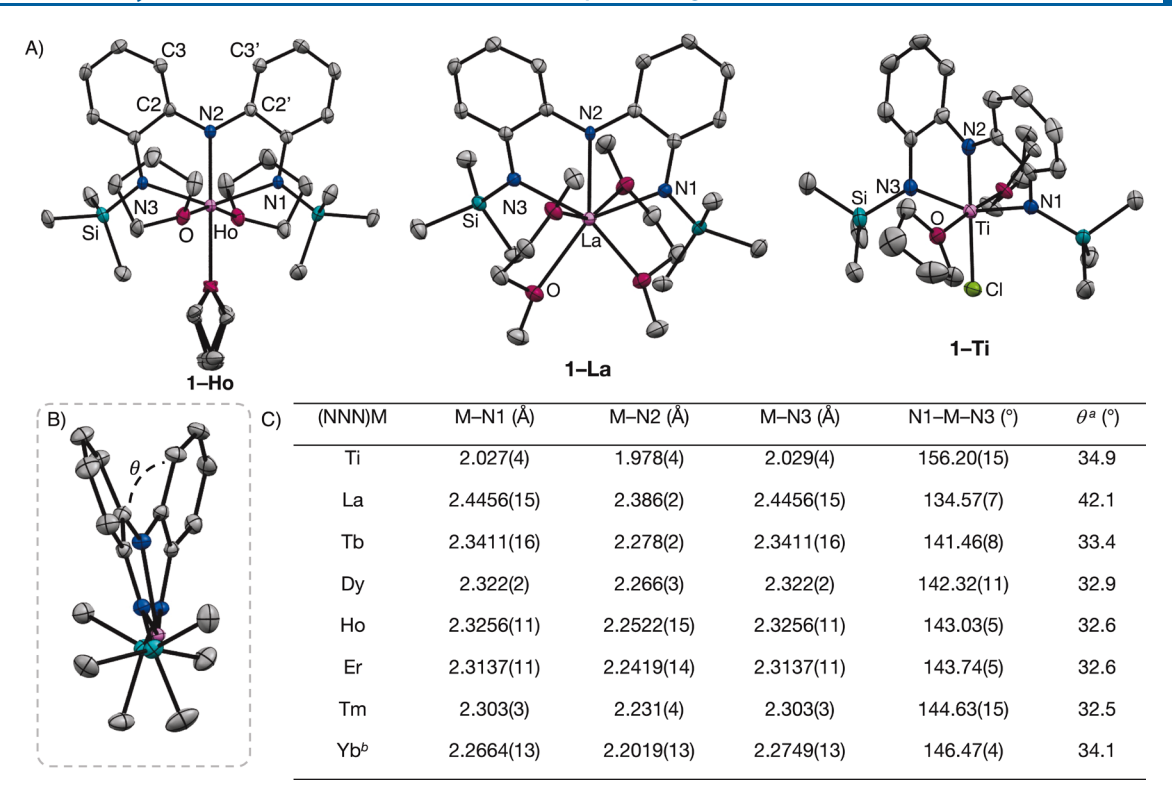


Figure 3. (A) Solid-state structures of 1–Ho (representative of 1–Ln), 1–La, and 1–Ti shown at the 50% thermal ellipsoid probability. Hydrogen atoms are omitted for clarity. Colors: blue, N; red, O; teal, Si; pink, M; gray, C; and green, Cl. (B) Ligand torsion angle ( $\theta = \angle C2-C3-C2'-C3'$ )<sup>a</sup> across N2. Bound THF ligands are omitted for clarity. (C) Selected bond distances and angles for complexes 1–Ln, 1–La, and 1–Ti. <sup>b</sup>1–Yb crystallizes with a Z'=2 in the asymmetric unit, and all values are reported as averages.

octahedral isostructural series of 1-Ln, seven-coordinate monocapped trigonal prismatic 1-La, and six-coordinate octahedral 1-Ti, as shown in Figure 3A, with selected bond distances and angles in Figure 3C. All complexes, with the exception of 1-Yb and 1-Ti, crystallized in the monoclinic space group C2/c. Complex 1-Yb crystallized in triclinic space group P-1, as does the previously reported 1-Sc. However, 1-Yb crystallized with a Z'=2 in the asymmetric unit, while 1-Sc possessed a Z'=1. Complex 1-Ti crystallized in monoclinic space group  $P2_1/n$ .

Across the series (La, Tb-Yb), both the equatorial (N1/N3) and apical (N2) Ln-N bond distances contract with the decreasing Ln³+ ionic radii from an average 2.4456–2.2664 (Ln-N1/N3) and 2.386–2.2019 (Ln-N2) Å. 59 Additionally, these bond distances trend well with the single bond covalent radii and charge densities (Figures S90–S93). 59–62 These structural trends are an indication that the metal-ligand bonding across the series of 1–Ln and 1–La is similar. Additionally, the C–C and C–N bond distances of the ligand in all 1–Ln, 1–La, and 1–Ti complexes are consistent with aromatic C–C bonds and C–N single bonds, emphasizing that the ligand is in the redox neutral state. The similar bond distances observed are indicative that the metal ion imposes little change in bond lengths on the ligand backbone.

However, across the full series (La<sup>3+</sup>, Tb<sup>3+</sup>–Lu<sup>3+</sup>, Sc<sup>3+</sup>, and Y<sup>3+</sup>) of rare earth complexes, the N1–M–N3 bond angle approaches linearity going from the largest ionic radii (La<sup>3+</sup>; 1.032 Å; 134.57°) to the smallest ionic radii (Sc<sup>3+</sup>; 0.745 Å; 154.03°). This is further supported by the observation of N1–M–N3 bond angles on 1–Ti (Ti<sup>4+</sup>; 0.605 Å; 156.20°) and previously reported 1–Zr (Zr<sup>4+</sup>; 0.720 Å; 148.30°). Additionally, while the identity of the metal minimally impacts bond

distances on the ligand backbone, there is a significant impact on the torsion angle. This torsion angle ( $\theta = \angle C2-C3-C2'-C3'$ ), defined in Figure 3B, varies drastically across the **1–Ln** series and trends strongly with the Pyykkö covalent radii ( $R^2 = 0.90$ ; Figure S96), indicating that the degree of covalency in the Ln–N bonds may impact the degree of ligand torsion observed.

**Cyclic Voltammetry.** To probe the electronic properties of complexes 1-Ln and 1-Ti, cyclic voltammetry (CV) studies were conducted in 0.25 M ["Bu<sub>4</sub>N]PF<sub>6</sub> THF solutions with 3 mM analyte at 298 K under an Ar atmosphere. CVs displaying the full electrochemical window were collected at 100 mV/s and are internally referenced to the FeCp2+/0 redox couple. A representative voltammogram displaying the general tris-(amido) ligand-based redox events for 1-Ln is shown in Figure 4A (see Supporting Information for individual voltammograms of each complex). All 1-Ln complexes exhibit two characteristic one-electron oxidation events ( $E_{pa}$  1 and 2) consistent with the semi-iminato and diazadiene states of the tris(amido) redox-active ligand, respectively. Three subsequent reduction events ( $E_{nc}$  1, 2, and 3) are observed across the rare earth series, with the exception of 1-Sc. A summary of all ligand-based redox events is listed in Table 1. Due to the poor solubility of 1-La in DME and the formation of a proposed dimeric species in other coordinating solvents (e.g. THF), CV experiments were unsuccessful.

The first single electron oxidation,  $E_{pa}$  1, for complexes 1–Ln and 1–Ti (see Supporting Information) was isolated and scan rate dependence studies were conducted from 50 to 1000 mV/s (Figure 4B). Complexes 1–Ln all exhibit an electrochemically quasi–reversible oxidation (see Supporting Information) ranging from -0.87 to -1.03 V vs  $FeCp_2^{+/0}$ , a

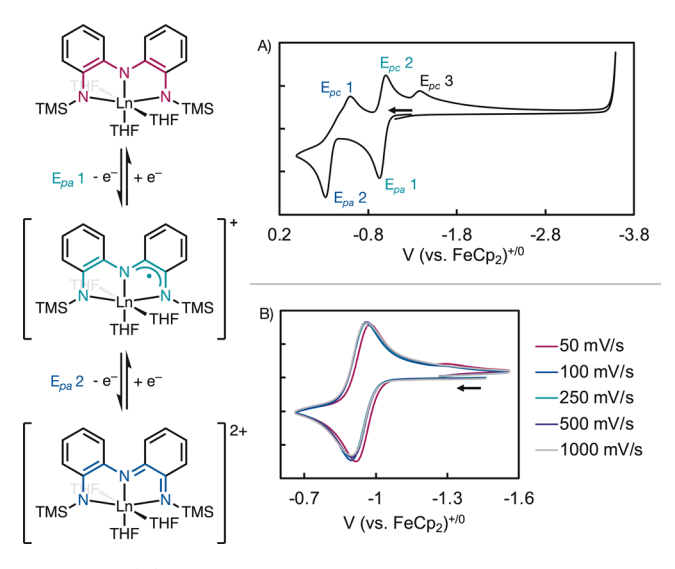


Figure 4. (A) Representative voltammogram displaying the tris-(amido)-based electrochemical processes for complexes 1-Ln (1-Dy shown). CVs were collected under Ar in 0.25 M [ $^nBu_4N$ ]PF<sub>6</sub> THF solutions with 3 mM analyte at 100 mV/s at 298 K. (B) Representative scan rate dependence studies on  $E_{pa}$  1 for complex 1-Ln (1-Dy shown) in 0.25 M [ $^nBu_4N$ ]PF<sub>6</sub> THF solutions with 3 mM analyte under Ar at ambient temperatures. Peak current potentials are normalized.

Table 1. Summary of Ligand-Based Redox Events of the 1-Ln Series

M(III)	E <sub>pa</sub> 1 (V)	$E_{pa}$ 2 (V)	E <sub>pc</sub> 1 (V)	E <sub>pc</sub> 2 (V)	$E_{pc}$ 3 (V)
Sc <sup>a,b</sup>	-0.82	-0.41	-0.46	-1.29	
$Y^a$	-0.92	-0.33	-0.61	-1.00	-1.32
Lua	-0.85	-0.26	-0.61	-0.92	-1.27
Tb	-0.96	-0.35	-0.60	-1.03	-1.40
Dy	-0.93	-0.32	-0.60	-1.00	-1.38
Ho	-0.91	-0.33	-0.61	-0.97	-1.31
Er	-0.87	-0.29	-0.58	-0.93	-1.25
Tm	-0.88	-0.31	-0.62	-0.94	-1.29
Yb	-1.03	-0.47	-0.76	-1.10	-1.45

"Voltammograms were recollected with applied iR compensation, and potentials were corrected from previous reports. "Complex 1-Sc features only two  $E_{pc}$  redox events. All potentials listed are from 0.25 M ["Bu<sub>4</sub>N]PF<sub>6</sub> THF solutions at 100 mV/s under Ar at ambient temperatures and referenced to the FeCp<sub>2</sub>\*-/0 redox couple.

difference of 160 mV. While in the full electrochemical window,  $E_{pc}$  3 was observed for all complexes, this event becomes minor across the series as the Ln3+ ion increased in size, where complex 1-Tb features the most electrochemically "reversible"-like redox process and 1-Yb features the least electrochemically "reversible"-like redox process based on peak current ratios (see Supporting Information Tables). The E<sub>pa</sub> 1 and  $E_{nc}$  2 peak-to-peak separation for all complexes shift moderately from 60 to 80 mV, only deviating slightly from 50 mV. Complex 1-Ti displays only a single, one-electron ligandbased oxidation event in the voltammogram at  $E_{pa} = 0.03 \text{ V}$  vs FeCp<sub>2</sub><sup>+/0</sup>, similarly to the previously reported  $\mathbf{1}-\mathbf{Zr}$  ( $\mathbf{E}_{pa}=0.10$  V vs FeCp<sub>2</sub><sup>+/0</sup>). Unlike  $\mathbf{1}-\mathbf{Zr}$ , complex  $\mathbf{1}-\mathbf{Ti}$  features two subsequent reduction events after the ligand-based oxidation. Scan rate dependence studies (Figure S5) highlight that the overall intensity of the second reduction event is scan rate dependent, where the ligand-based oxidation is electrochemically quasi-reversible at faster scan rates based on peak current ratios (Supporting Information Tables).

Upon excluding complexes 1–Sc and 1–Ti from the series (as their CVs and electronic properties are significantly different from those of the rest of the rare earth series), a good trend was observed by plotting (Figure 5) the previously

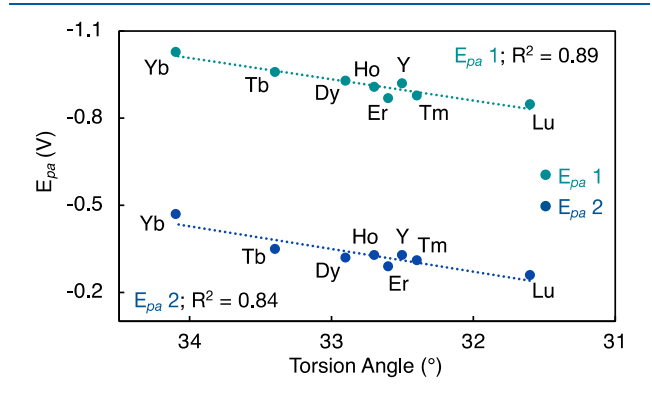


**Figure 5.** Oxidation potentials  $E_{pa}$  1 and 2 for complexes 1–Y, 1–Lu, and 1–Ln plotted against the observed torsion angle  $(\theta)$  in the solid state.

discussed ligand torsion angle against the oxidation potentials ( $E_{pa}$  1  $R^2$  = 0.89,  $E_{pa}$  2  $R^2$  = 0.84). These trends allude to a potential disruption in the aromatic  $\pi$ –conjugation, where the complexes with a smaller ligand torsion angle result in stronger conjugation, leading to slightly harsher oxidation potentials for both  $E_{pa}$  1 and 2.

In addition to the tris(amido) redox properties observed, complexes 1–Ti, 1–Tb, and 1–Yb all possess metal-based redox events (Figure 6). Complex 1–Ti features an electro-

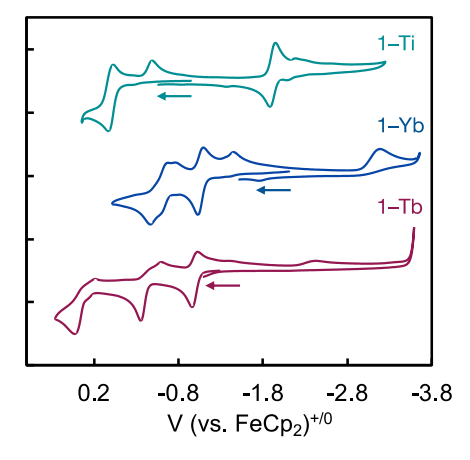


Figure 6. Stacked CV of complexes 1–Ti, 1–Yb, and 1–Tb feature metal-based redox events. CVs collected under Ar in 0.25 M ["Bu<sub>4</sub>N]PF<sub>6</sub> THF solutions with 3 mM analyte at 100 mV/s at 298 K.

chemically quasi-reversible reduction based on peak current ratios and scan rate studies (see Supporting Information Tables) observed at  $E_{pc} = -1.95$  V vs  $FeCp_2^{+/0}$ . This reduction event was assigned as the Ti(III/IV) redox event. Reports of Ti(III/IV) redox couples are scarce for complexes bearing multiple amido donors. However, the complex  $Ti^{IV}(\kappa^2 - Me_3SiNCH_2CH_2NSiMe_3)_2$  displayed a Ti(III/IV) redox event at -2.3 V vs  $FeCp_2^{+/0}$  in THF.  $^{63,64}$  This potential deviates by 350 mV, which could be a result of the more electron-rich nature of the reported homoleptic amide complex

in comparison to complex 1-Ti. In contrast, no metal-based reduction events were observed in previously reported complex 1-Zr.

With electronic configurations of 4f8 and 4f13 respectively, 1-Tb and 1-Yb can readily access a half-filled set (Tb<sup>4+</sup>; 4f<sup>7</sup>) and filled set of 4f orbitals (Yb<sup>2+</sup>; 4f<sup>14</sup>). Complex 1-Tb features an electrochemically irreversible oxidation at  $E_{pa}$ 0.43 V vs FeCp<sub>2</sub><sup>+/0</sup>, nearing the THF solvent window, assigned as the Tb(III/IV) redox event. Observation of Tb<sup>4+</sup> redox events has previously been limited to terbium oxides, fluorides, and concentrated aqueous carbonate solutions due to the high redox potentials associated with this oxidation. 65,66 Most Tb(III/IV) redox events have been observed primarily in ["Bu<sub>4</sub>N]BAr<sup>F</sup><sub>4</sub> [BAr<sup>F</sup><sub>4</sub> = tetrakis(pentafluorophenyl)borate] dichloromethane solutions at potentials ranging from  $E_{pa} = 0.078$  to 0.582 V vs  $FeCp_2^{+/0.66}$  While solvent and electrolyte differences restrict a direct comparison, the overall harsh oxidation potentials observed for accessing Tb4+ are in line with the observed oxidation potential for complex 1-Tb. Complex 1-Yb features an electrochemically irreversible reduction event at  $E_{pc} = -3.12 \text{ V}$  vs  $\text{FeCp}_2^{+/0}$ , nearing the THF solvent window. Observation of Yb(II/III) redox events in lanthanide complexes is far more common, and the observed reduction potential in 1-Yb is in accordance with other reported Yb3+ complexes.41 Scan rate dependence studies (Figure S79) from 50 to 1000 mV/s displayed that the Yb(II/ III) reduction remained irreversible.

Synthesis of 2-Ln, 2-La, and 2-Ti. Initial electrochemical studies on the previously reported tris(amido) complexes (1-Sc, 1-Y, 1-Lu, and 1-Zr) displayed a single electron oxidation of the ligand backbone to generate the semiiminato (ligand radical) redox state. The semi-iminato complexes were previously identified as relevant intermediates in the established alkyl-alkyl cross-coupling catalysis. 54-56 Isolation of the reported semi-iminato complexes (2-Sc, 2-Y, and 2-Lu) involved treatment of the redox neutral complex with an appropriate oxidant, such as PhICl2 yielding PhI. Additionally, during these studies, CuCl was found to be a convenient, mild one-electron oxidant, where Cu0 could be removed from the reaction mixture via filtration.<sup>67</sup> These synthetic methods were applied interchangeably to the series of 1-Ln complexes (Figure 7), where complexes 2-Ln were isolated as dark green powders in yields of 75-80%. The use of CuCl to oxidize 1-La resulted in the generation of an unknown species; however, PhICl2 as an oxidant generated 2-La as a green powder in 80% yield. Complexes 2-Ln and 2-La exhibit greater overall solubility (slightly soluble in hydrocarbons, soluble in aromatic and ethereal solvents) compared to 1-Ln and 1-La. <sup>1</sup>H NMR, EPR, and UV-vis spectroscopic methods, along with DFT calculations (vide infra), are consistent with the structural assignments and the presence of an organic radical delocalized across the ligand backbone. Due to the harsh oxidation potential of complex 1-Ti (vide supra), one equivalent of PhICl<sub>2</sub> was used. Isolation of 2-Ti proved to be difficult due to light and thermal sensitivity, resulting in all studies being conducted in situ.

**NMR Spectroscopy.** Previous  $^{1}$ H NMR studies on **1–Sc** in aromatic solvents displayed the loss of a THF ligand in solution, resulting in a mixture of the tris(THF) and bis(THF) complexes.  $^{54}$  To maintain complete solvation on each of the **1–Ln/1–Ti** and **2–Ln/2–Ti** complexes, all  $^{1}$ H NMR studies were conducted in THF– $d_{8}$ . Complexes **1–Ln** and **1–Ti** exhibit  $C_{2y}$  symmetry in THF– $d_{8}$  solutions, where four

Figure 7. Oxidation of tris(amido) complexes.

Мe

aromatic protons and one TMS resonance are observed, all integrating to 2:2:2:2:18 protons, respectively (see Supporting Information for each individual spectra). Crystals of 1–La were dissolved in hot toluene– $d_8$ , and  $C_{2\nu}$  symmetry was also observed in the <sup>1</sup>H NMR spectrum (Figure S14). Relative integrations are consistent with two DME molecules bound to the La<sup>3+</sup> center.

Upon chemical oxidation, we were interested in determining whether any coordination changes were observed, given the highly electropositive nature of these complexes. Interestingly, compared to their diamagnetic d<sup>0</sup> metal counterparts (2-La, 2-Lu, 2-Sc, 2-Y, and 2-Zr) where only a broad resonance corresponding to the TMS protons was observed, all five resonances are observed with the 2-Ln complexes. Complexes **2–Ln** exhibit  $C_{2\nu}$  symmetry in THF– $d_8$  solutions, where 4 aromatic protons and one TMS resonance are observed, all integrating to 2:2:2:18 protons, respectively (see Supporting Information for individual spectra). While no changes were observed in the pattern of the spectra (i.e., number of signals and relative integrations) from 1-Ln, the chemical shift ranges for 2-Ln were found to change dramatically. For example, complex 1-Yb ( $\delta$  -4.64 to -43.0 ppm) displays a large change in chemical shift upon oxidation, where 2-Yb ( $\delta$  -14.8 to -166.6 ppm) is significantly shifted in the <sup>1</sup>H NMR spectrum. Due to thermal and light sensitivity, 2-Ti was not isolated. The <sup>1</sup>H NMR spectrum of the *in situ* oxidation using PhICl<sub>2</sub> revealed the disappearance of 1-Ti and the growth of aromatic resonance peaks of the byproduct PhI.

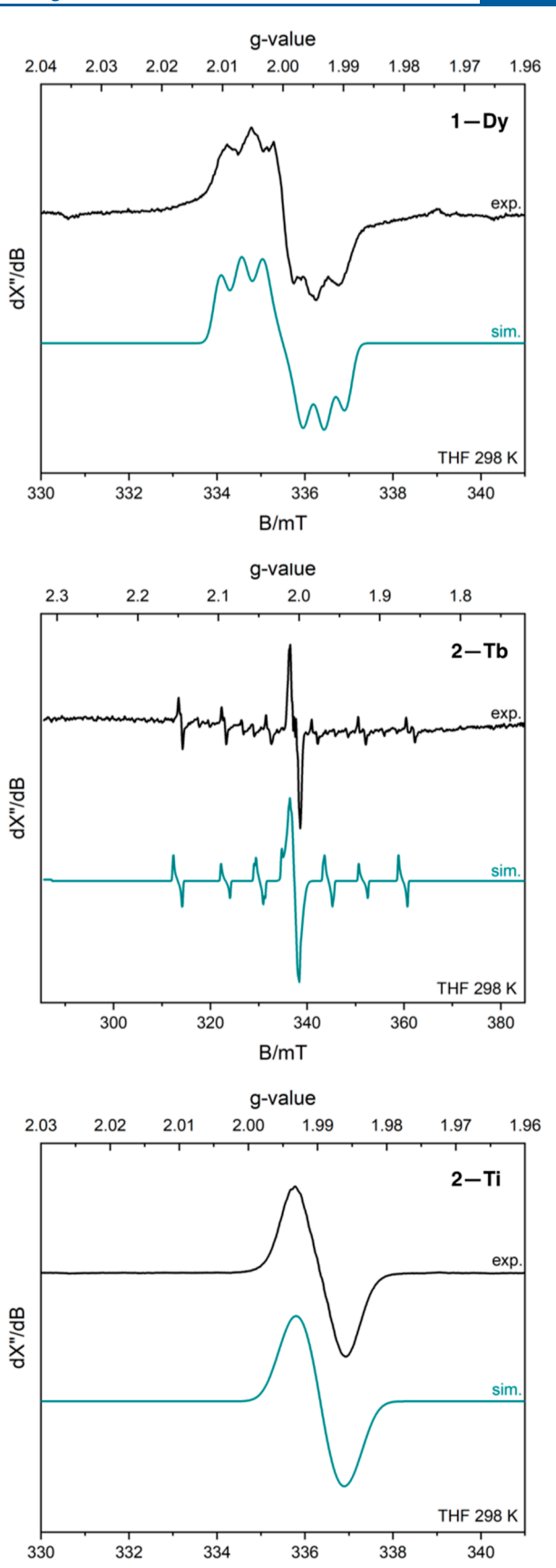
**EPR.** X-band EPR spectroscopy was used to elucidate the nature of the unpaired electrons in the paramagnetic lanthanide complexes **1–Ln** and the radicals formed in the chemically oxidized complexes, **2–Ln**, **2–La**, and **2–Ti**. While most lanthanide complexes are paramagnetic in nature, the 4f-orbital electrons experience rapid relaxation effects that can prevent EPR spectra from being observed above 4.2 K. <sup>23,68</sup> Surprisingly, an EPR spectrum of **1–Dy** was obtained by using a concentrated solution of the complex in THF at room temperature. This gave an isotropic signal  $g_{iso} = 2.0035$  with

hyperfine coupling to the dysprosium center  $[A_{iso}]^{(163)}$ Dy, n =1) = 248.98 MHz] and weak superhyperfine coupling to two inequivalent nitrogen atoms in the tris(amido) ligand  $[A_{iso}]$  $(^{14}N, n = 1) = 2.3 \text{ MHz}, A_{iso} (^{14}N, n = 1) = 12.1 \text{ MHz}].$  The superhyperfine coupling to the ligand is likely due to the proximity of the nitrogen atoms to the metal center. 54-56 The spectrum of 2-Ti displays a single isotropic signal with a  $g_{iso}$  = 1.998. The spectra of the singly oxidized lanthanide complexes 2-Ln and 2-La all show similar signals that differ greatly from that of 2-Ti with signals present throughout an expanded sweep width of the magnetic field. Simulations of these spectra (2-Tb shown in Figure 8) reveal a signal corresponding to a radical delocalized around the ligand [ $g_{iso} = 2.0025$ ,  $A_{iso}$  ( $^{14}N$ , n= 2) = 200.3,  $A_{iso}$  (<sup>14</sup>N, n = 1) = 654.6, and  $A_{iso}$  (<sup>1</sup>H, n = 1) = 10.3]. The *g*-value of these spectra are all close to that of a free radical (g = 2.0023), and the identity of the lanthanides has little to no effect on the resulting spectra. 69 This highlights the organic character of the radical and the absence of any spin-spin interactions.

**Electronic Absorption Spectroscopy.** The electronic absorption spectra of complexes **1–Ln** and **1–Ti** (Figure S10) were collected in 0.1 mM THF solutions and are shown in Figure 9A. All **1–Ln** complexes, where most are various shades of yellow (with the exception of green **1–Yb**), were dominated by intense ligand aromatic  $\pi$ – $\pi$ \* charge transfer bands ( $\varepsilon$  > 9000 M<sup>-1</sup> cm<sup>-1</sup>) observed in the UV region below 400 nm. Additionally, a weak charge transfer band ( $\varepsilon$  > 200 M<sup>-1</sup> cm<sup>-1</sup>) was observed in all **1–Ln** complexes near 400 nm. This transition is most likely a very weak ligand to metal charge transfer band based on the low extinction coefficients and absorbances in the far UV region. Similarly, the deep green complex **1–Ti** exhibited strong  $\pi$ – $\pi$ \* charge transfer bands ( $\varepsilon$  > 8000 M<sup>-1</sup> cm<sup>-1</sup>), followed by a weak LMCT band starting at 590 nm ( $\varepsilon$  > 2000 M<sup>-1</sup> cm<sup>-1</sup>) (Figure S10).

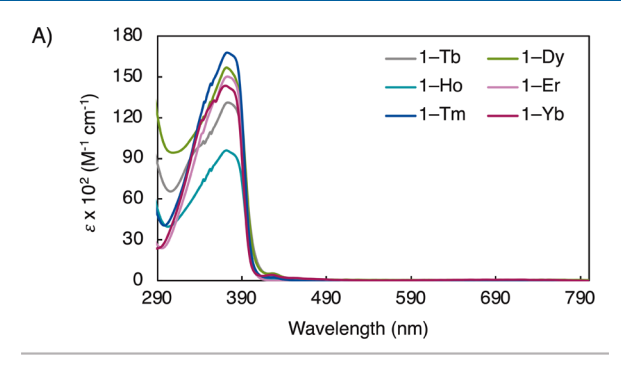
Increasing concentrations from 0.1 to 20 mM solutions allowed for the observance of weak ( $\varepsilon=2-10~{\rm M}^{-1}~{\rm cm}^{-1}$ ) parity-forbidden 4f to 4f transitions for complexes 1–Tb, 1–Dy, 1–Ho, 1–Er, and 1–Tm all ranging from 470–1600 nm (Figure S91). Complex 1–Yb, a vivid emerald green, displayed several charge transfer bands from 660–690 nm ( $\varepsilon=127~{\rm M}^{-1}~{\rm cm}^{-1}$ ), 929 nm ( $\varepsilon=56~{\rm M}^{-1}~{\rm cm}^{-1}$ ), and 1003 nm ( $\varepsilon=185~{\rm M}^{-1}~{\rm cm}^{-1}$ ) in the visible–near-infrared (NIR) region that are consistent with various spin-allowed 4f to 5d electronic transitions for Yb<sup>3+</sup> complexes (Figure S82). Unfortunately, due to the air sensitivity of these complexes, oxidation impurities of the tris(amido) ligand were observed with the broad signal near 1100 nm at such high concentrations.

Upon chemical oxidation to generate the semi-iminato state of the tris(amido) ligand, all complexes were dark green in THF solutions. Spectra were collected in 0.1 mM THF solutions from 270-1600 nm. More concentrated solutions were used to attempt observation of parity-forbidden 4f to 4f electronic transitions; however, due to oversaturation of the detector, no discernible data was obtained. Complexes 2-Ln featured similar spectra (Figure 9B), where three major charge transfer bands were observed in the UV (270-450 nm) region of the spectrum with extinction coefficients ranging from about  $\varepsilon = 6000 - 15,000 \text{ M}^{-1} \text{ cm}^{-1}$ . Weaker bands ( $\varepsilon < 3000 \text{ M}^{-1}$ cm<sup>-1</sup>) were observed in the visible region, followed by an intense, broad charge transfer band ( $\varepsilon > 3000 \text{ M}^{-1} \text{ cm}^{-1}$ ) in the NIR, a diagnostic signal observed in previously reported rare earth and early transition metal complexes in the semiiminato state of the tris(amido) ligand. 52-56 Complex 2-Ti



**Figure 8.** Experimental (black) and simulated (teal) X-band EPR spectra of complexes **1–Dy**, **2–Tb**, and **2–Ti**. EPR spectra were collected in THF at 298 K. See Supporting Information for full details.

B/mT



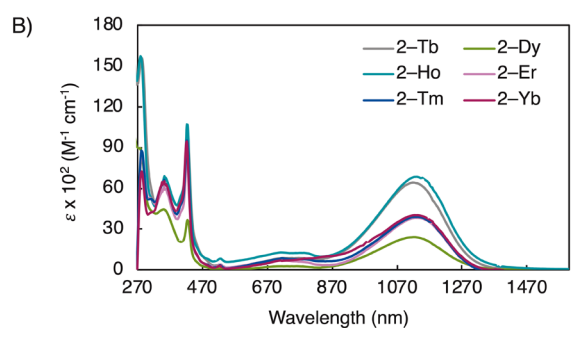


Figure 9. UV–vis/NIR spectra of complexes (A) 1–Ln and (B) 2–Ln. Spectra were collected in 0.1 mM THF solutions under Ar or  $\rm N_2$  at 298 K.

presented a blue-shifted ligand–based aromatic  $\pi-\pi^*$  charge transfer band at 300 nm ( $\varepsilon$  > 10,000 M $^{-1}$  cm $^{-1}$ ) and a broad band around 400 nm ( $\varepsilon$  < 4000 M $^{-1}$  cm $^{-1}$ ).

To maintain the monomeric structure of 1–La and 2–La, analysis of 0.1 mM solutions was conducted in DME (Figure S19). Complexes 1–La and 2–La exhibited very similar UV–vis/NIR spectra compared to their most closely related analogue, 1–Lu and 2–Lu. <sup>56</sup> In addition to a ligand-based aromatic  $\pi$ – $\pi$ \* charge transfer band ( $\varepsilon$  > 9000 M<sup>-1</sup> cm<sup>-1</sup>) observed in the UV region, a small shoulder was observed. The lower extinction coefficient and additional shoulder band may be a result of the strong ligand torsion observed in the solid-state structure, disrupting conjugation of the aromatic  $\pi$ –electron density.

Computational Studies. DFT calculations were performed to further probe the electronic characteristics of these novel complexes. Geometry optimizations and energy calculations were carried out using hybrid functional B3LYP with basis sets 6-31g\* for organic atoms and def2-TZVP for metals.34,70 4f-in-core effective core potentials were applied for 1-Ln and 1-La, and the polarizable continuum model was used to account for THF solvation effects in complexes 1-Ln and 1-Ti. All 1-Ln complexes show the same frontier orbitals,  $(173\alpha)$  HOMO and  $(174\alpha)$  LUMO, with relatively uniform HOMO-LUMO energy gaps (81.2-91.7 kcal/mol). The absence of 4f-electrons in diamagnetic complex 1-La resulted in lower energy frontier orbitals, (147 $\alpha$ ) HOMO and (148 $\alpha$ ) LUMO, and a smaller energy gap of 69.7 kcal/mol. Additionally, 1–Ti presented frontier orbitals, (151 $\alpha$ ) HOMO and  $(152\alpha)$  LUMO, with a much higher energy gap of 215.7 kcal/mol. This expanded HOMO-LUMO energy gap aligns with the increased potential required to observe singly oxidized complex 2-Ti by CV.

Population analysis of the  $\alpha$  orbitals was conducted to elucidate the metal contribution to the HOMO and LUMO.

Complexes 1–Ln, 1–La, and 1–Ti contain minor percentages of metal character in the HOMO (0–6%), while an increase of metal character is reflected in the LUMO (66–100%). Following single-electron oxidation, a notable difference is observed between 2–Dy and 2–Ti. The metal character in the LUMO for 2–Ti stayed relatively consistent (80%), while the metal character of the LUMO for 2–Dy greatly diminished from 66 to 7% following the oxidation. This may be reflective of the difference between the covalent and ionic bonding nature of early transition metals and lanthanides.

Spin density plots of neutral 1-Dy and singly oxidized 2-Ti, 2-La, and 2-Dy (Figure 10) demonstrate the effects that

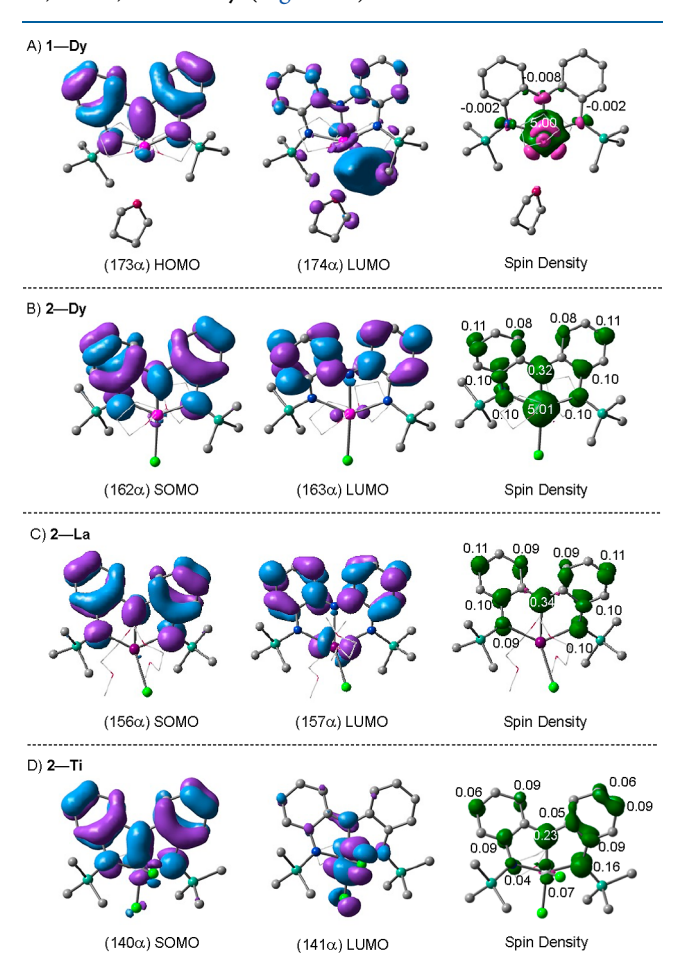


Figure 10. Molecular orbital plots (isovalue = 0.03) and spin density plots (isovalue = 0.00045) for complexes (A) 1–Dy, (B) 2–Dy, (C) 2–La, and (D) 2–Ti (see Supporting Information for details).

4f—electrons can have on the system. As expected, complex 1—Dy has most of its spin density at the lanthanide center; however, sharing of the spin density to the nitrogen atoms on the ligand is also observed. This interaction supports the ligand character observed in the EPR spectrum of 1—Dy. The spin density of 2—Dy is spread throughout the metal and ligand, corresponding to unpaired 4f—electrons as well as a ligand-based radical. Furthermore, 2—Ti and 2—La exhibit plots similar to those of the previously reported 2—Sc complex with spin density shared throughout the ligand backbone.

Alkyl-Alkyl Cross-Coupling. The catalytic efficacy of complexes 1-Ln, 1-La, and 1-Ti was determined in duplicate trials where 10 mol % of each complex was used in the presence of equimolar amounts of nucleophilic trans-

metalating reagent, benzyl zinc bromide, and electrophilic/oxidizing coupling partner, (1–bromoethyl)benzene. Previous kinetic studies with 1–Y demonstrated that the electrophile is involved in the rate-determining step; therefore, reaction monitoring of the consumption of (1–bromoethyl)benzene was conducted to determine the initial rate of the reaction over a period of 6 h.<sup>55</sup> Additional time points were collected to determine the final yields of the cross-coupled product at 48 h (see Supporting Information for reaction monitoring plots). The reaction monitoring plot for complex 1–Dy is shown in Figure 11. Complex 1–Ti featured the slowest rate and the

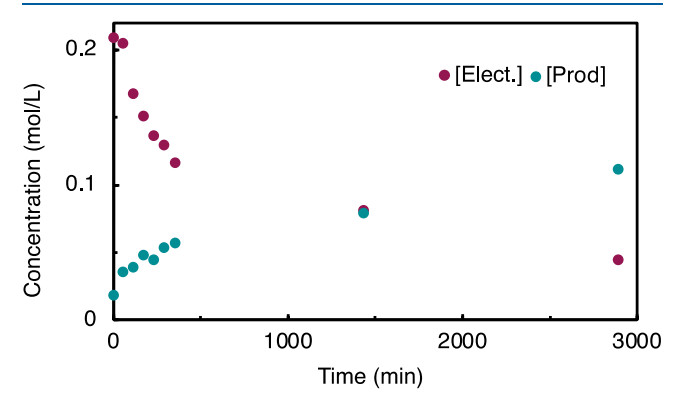


Figure 11. Plot monitoring the reaction progress of the cross-coupling of (1-bromoethyl)benzene with benzyl zinc bromide catalyzed by 1-Dy. Data are an average of duplicate runs. [Elect.] is the concentration of (1-bromoethyl)benzene in mol/L.

lowest yield, similar to those of its previously reported congener 1–Zr. The average initial rate and yield of the cross-coupled product are displayed in Figure 12.

In general, the rates across the entire 1-La and 1-Ln series were comparable, and therefore, by analogy, we hypothesize

Ph ZnBr + (1 equiv.)	Br Ph Me (1 equiv.)	10 mol% <b>1–M</b> THF–d <sub>8</sub> 22 °C, 48 h	Ph
1-M	,	e x 10 <sup>-6</sup> (M/s)	Yield

1-M	Rate x 10 <sup>-6</sup> (M/s)	Yield
Sc <sup>a</sup>	-1.67	77%
Υa	<b>-</b> 2.27	58%
Lu <sup>a</sup>	-2.91	50%
Ti	-1.31	18%
La	-4.00	51%
Tb	-3.94	51%
Dy	-4.63	56%
Но	-3.88	55%
Er	<b>-</b> 3.73	53%
Tm	-4.91	48%
Yb	-3.60	51%

**Figure 12.** Catalytic  $C(sp^3)-C(sp^3)$  cross-coupling catalysis using **1**–**M** with summarized initial rates and yields. Data are shown as the average of duplicate runs. <sup>a</sup>Initial rates and yields are previously reported.

that a common mechanism is likely observed as previously studied using 1-Y (Figure S97). 55,71,72 Initial transmetalation with benzyl zinc bromide to precatalyst 1-Ln generates an anionic 1-Ln(Bn) benzyl complex. The SET/halogen atom abstraction event via a non-classical oxidative addition generates the semi-iminato redox state of the tris(amido) ligand and a benzylic radical from (1-bromoethyl)benzene. An outer sphere radical attack (S<sub>H</sub>2) from the benzylic radical to the Ln-Bn bond generates the cross-coupled product and reduces the ligand back to the redox neutral tris(amido) state, where an anionic tris(amido) lanthanide-bromide complex is maintained. A second transmetalation regenerates the active 1-Ln(Bn) complex, turning over the reaction. No correlation with the initial rate of the reaction and the  $E_{pa}$  1 or 2 redox potentials was observed. Despite 1-La undergoing ligand exchange in the presence of coordinating solvents (vide supra), no deleterious effects were observed during catalysis. Despite the comparable rate to 1-Sc, complex 1-Ti produced poor yields of the cross-coupled product. This is proposed to be a direct effect of the harsh E<sub>pa</sub> 1 oxidation potential, similar to that of 1-Zr.

# CONCLUSIONS

An isostructural series of six-coordinate complexes 1–Ln, six-coordinate 1–Ti, and seven-coordinate 1–La was successfully synthesized. Complexes 1–Ln, 1–La, and 1–Ti were studied extensively through multiple methods (XRD, electronic absorption spectroscopy, CV, and DFT). Complexes 1–Ln were found to exhibit very similar structural features and electronic properties, implying that the bonding and electronic structure are similar across the series. Additionally, the single electron chemical oxidation of the ligand backbone was conducted, leading to the isolation of another series of complexes, 2–Ln and 2–La. Complex 2–Ti was found to be unstable in solution and in the solid state over extended periods of time, leading to all studies being conducted in situ.

All complexes studied by CV were found to possess at least one ligand-based single electron oxidation event in their voltammograms. Interestingly, with complexes 1–Ln, the ligand-based oxidation events ( $E_{\rm pa}$  1 and 2) were found to correlate with the ligand torsion angle ( $\theta$ ) observed in the solid state. As the torsion angle ( $\theta$ ) increased, the oxidation potentials were found to be milder. This trend is indicative that as the  $\pi$ -conjugation is disrupted with increased torsion angles, the oxidation of the redox-active tris(amido) ligand becomes more facile. In addition to ligand-based redox events, metal-based redox processes were observed for complexes 1– Tb, 1–Yb, and 1–Ti.

The singly oxidized complexes 2–Ln, 2–La, and 2–Ti presented EPR spectra indicative of semi-iminato complexes. Additionally, fully reduced 1–Dy exhibited an EPR spectrum with radical character shared between the metal and the ligand. These results were further supported with DFT calculations of the complexes.

Lastly, all tris(amido) complexes were found to be competent catalysts for alkyl—alkyl cross-coupling in the presence of transmetalating reagent, benzyl zinc bromide, and electrophilic/oxidizing coupling partner, (1—bromoethyl)-benzene. All 1—Ln complexes were found to produce similar yields after 48 h, as well as possess similar initial rates of their reactivity. Due to their similar kinetic reaction profile and previously conducted mechanistic studies, <sup>55</sup> 1—Ln is believed

to follow the same mechanism of previously reported complexes (1-Sc, 1-Y, and 1-Lu).

In summary, a series of tris(amido) complexes were synthesized and characterized thoroughly. These complexes, normally known for their lack of redox chemistry, were found to successfully promote  $C(sp^3)-C(sp^3)$  cross-coupling catalysis through the use of a RAL. Further reactivity involving one-and two-electron processes is currently being explored.

## ASSOCIATED CONTENT

# Supporting Information

The Supporting Information is available free of charge at https://pubs.acs.org/doi/10.1021/acs.inorgchem.4c01909.

Synthesis and characterization; stoichiometric transmetalation studies using complex 1–Ho and BnZnBr; crystallographic bond metrics for 1–Ti, 1–La, and 1–Ln; CV recollection of 1–Sc, 1–Y, and 1–Lu; NIR spectra of 1–Ln; trend analysis of complexes 1–Ln; and proposed mechanism for  $C(sp_3)-C(sp_3)$  cross-coupling (PDF)

#### **Accession Codes**

CCDC 2353879–2353886 contain the supplementary crystallographic data for this paper. These data can be obtained free of charge via <a href="www.ccdc.cam.ac.uk/data\_request/cif">www.ccdc.cam.ac.uk/data\_request/cif</a>, or by emailing <a href="data\_request@ccdc.cam.ac.uk">data\_request/cif</a>, or by contacting The Cambridge Crystallographic Data Centre, 12 Union Road, Cambridge CB2 1EZ, UK; fax: +44 1223 336033.

#### AUTHOR INFORMATION

# **Corresponding Author**

Courtney C. Roberts — Department of Chemistry, University of Minnesota, Minneapolis, Minnesota 55455, United States; orcid.org/0000-0001-8177-4013; Email: ccrob@umn.edu

## **Authors**

Nicholas A. Garcia — Department of Chemistry, University of Minnesota, Minneapolis, Minnesota 55455, United States; orcid.org/0000-0001-6809-2966

Victoria C. Tafuri — Department of Chemistry, University of Minnesota, Minneapolis, Minnesota 55455, United States; orcid.org/0000-0003-1486-2018

Rana B. Abdu – Department of Chemistry, University of Minnesota, Minneapolis, Minnesota 55455, United States; orcid.org/0009-0003-5607-9539

Complete contact information is available at: https://pubs.acs.org/10.1021/acs.inorgchem.4c01909

# **Author Contributions**

\*N.A.G. and V.C.T. contributed equally.

#### **Funding**

Financial support was provided in part by the NSF Award CHE-2237586. R.B.A. acknowledges the NSF-GRFP Award #2237827 and the Graham N. Gleysteen Departmental First Year Fellowship.

# Notes

The authors declare no competing financial interest.

#### ACKNOWLEDGMENTS

The authors would like to acknowledge the Blank and Gladfelter groups for equipment used to obtain UV-vis/NIR

data. X—ray diffraction experiments were performed using a crystal diffractometer acquired through an NSF—MRI award (CHE1229400) in the X—ray laboratory supervised by Dr. Victor G. Young. The authors would also like to acknowledge Alex Lovstedt for assistance with XRD collection and structure refinements. The authors also acknowledge Dr. Roman G. Belli for previous work conducted on early transition metal complexes bearing the tris(amido) ligand used in this work.

# REFERENCES

- (1) Ephritikhine, M. Recent Advances in Organoactinide Chemistry As Exemplified by Cyclopentadienyl Compounds. *Organometallics* **2013**, 32 (9), 2464–2488.
- (2) Murugesu, M.; Schelter, E. J. Not Just Lewis Acids: Preface for the Forum on New Trends and Applications for Lanthanides. *Inorg. Chem.* **2016**, *55* (20), 9951–9953.
- (3) Coughlin, E. J.; Zeller, M.; Bart, S. C. Neodymium(III) Complexes Capable of Multi-Electron Redox Chemistry. *Angew. Chem., Int. Ed.* **2017**, 56 (40), 12142–12145.
- (4) Weber, M. J. Lanthanide and Actinide Lasers. In Lanthanide and Actinide Chemistry and Spectroscopy; ACS Symposium Series; American Chemical Society, 1980; Vol. 131, pp 275–311..ACS Symposium Series
- (5) Woodruff, D. N.; Winpenny, R. E. P.; Layfield, R. A. Lanthanide Single-Molecule Magnets. *Chem. Rev.* **2013**, *113* (7), 5110–5148.
- (6) Xia, S.-B.; Li, F.-S.; Shen, X.; Li, X.; Cheng, F.-X.; Sun, C.-K.; Guo, H.; Liu, J.-J. A Lanthanide-Based Coordination Polymer as Lithium Ion Battery Anode with High Cyclic Stability. *Mater. Lett.* **2019**, 238, 171–174.
- (7) Pellissier, H. Recent Developments in Enantioselective Lanthanide-Catalyzed Transformations. *Coord. Chem. Rev.* **2017**, 336, 96–151.
- (8) Qin, X.; Liu, X.; Huang, W.; Bettinelli, M.; Liu, X. Lanthanide-Activated Phosphors Based on 4f-5d Optical Transitions: Theoretical and Experimental Aspects. *Chem. Rev.* **2017**, *117* (5), 4488–4527.
- (9) MacKenzie, L. E.; Pal, R. Circularly Polarized Lanthanide Luminescence for Advanced Security Inks. *Nat. Rev. Chem* **2020**, 5 (2), 109–124.
- (10) Teo, R. D.; Termini, J.; Gray, H. B. Lanthanides: Applications in Cancer Diagnosis and Therapy. *J. Med. Chem.* **2016**, 59 (13), 6012–6024.
- (11) Bottrill, M.; Kwok, L.; Long, N. J. Lanthanides in Magnetic Resonance Imaging. *Chem. Soc. Rev.* **2006**, 35 (6), 557–571.
- (12) Harvey, P.; Kuprov, I.; Parker, D. Lanthanide Complexes as Paramagnetic Probes for 19F Magnetic Resonance. *Eur. J. Inorg. Chem.* **2012**, 2012 (12), 2015–2022.
- (13) Zhang, M.; Qu, Z.; Han, C.-M.; Lu, L.-F.; Li, Y.-Y.; Zhou, T.; Shi, G. Time-Resolved Probes and Oxidase-Based Biosensors Using Terbium(Iii)-Guanosine Monophosphate-Mercury(Ii) Coordination Polymer Nanoparticles. *Chem. Commun.* **2014**, *50* (85), 12855–12858
- (14) Dam, H. H.; Reinhoudt, D. N.; Verboom, W. Multicoordinate Ligands for Actinide/Lanthanide Separations. *Chem. Soc. Rev.* **2007**, 36 (2), 367–377.
- (15) Higgins, R. F.; Ruoff, K. P.; Kumar, A.; Schelter, E. J. Coordination Chemistry-Driven Approaches to Rare Earth Element Separations. *Acc. Chem. Res.* **2022**, *55* (18), 2616–2627.
- (16) Cheisson, T.; Schelter, E. J. Rare Earth Elements: Mendeleev's Bane, Modern Marvels. *Science* **2019**, *363* (6426), 489–493.
- (17) Janicki, R.; Mondry, A. Structural and Thermodynamic Aspects of Hydration of Gd(III) Systems. *Dalton Trans.* **2019**, 48 (10), 3380–3391.
- (18) Sun, T.; Gao, Y.; Du, Y.; Zhou, L.; Chen, X. Recent Advances in Developing Lanthanide Metal-Organic Frameworks for Ratiometric Fluorescent Sensing. *Front. Chem.* **2021**, *8*, 624592.
- (19) Zhou, J.; Leaño, J. L., Jr; Liu, Z.; Jin, D.; Wong, K.-L.; Liu, R.-S.; Bünzli, J. G. Impact of Lanthanide Nanomaterials on Photonic Devices and Smart Applications. *Small* **2018**, *14* (40), 1801882.

- (20) Chen, X.; Sun, T.; Wang, F. Lanthanide-Based Luminescent Materials for Waveguide and Lasing. *Chem. Asian J.* **2020**, *15* (1), 21–33.
- (21) Zhang, P.; Guo, Y.-N.; Tang, J. Recent Advances in Dysprosium-Based Single Molecule Magnets: Structural Overview and Synthetic Strategies. *Coord. Chem. Rev.* **2013**, 257 (11–12), 1728–1763.
- (22) Rinehart, J. D.; Long, J. R. Exploiting Single-Ion Anisotropy in the Design of f-Element Single-Molecule Magnets. *Chem. Sci.* **2011**, 2 (11), 2078–2085.
- (23) Lanthanide and Actinide Chemistry.
- (24) Greenwood, N. N.; Earnshaw, A. Chemistry of the Elements, 2nd ed.; Butterworth-Heinemann: Oxford, 2006.
- (25) Jaroschik, F.; Momin, A.; Nief, F.; Le Goff, X.; Deacon, G. B.; Junk, P. C. Dinitrogen Reduction and C–H Activation by the Divalent Organoneodymium Complex [(C<sub>5</sub>H<sub>2</sub>tBu<sub>3</sub>)<sub>2</sub>Nd(μ–I)K-([18]crown–6)]. *Angew. Chem., Int. Ed.* **2009**, 48 (6), 1117–1121.
- (26) Nief, F. Non-Classical Divalent Lanthanide Complexes. *Dalton Trans.* **2010**, *39* (29), *6589*–6598.
- (27) Momin, A.; Bonnet, F.; Visseaux, M.; Maron, L.; Takats, J.; Ferguson, M. J.; Le Goff, X. F.; Nief, F. Synthesis and Structure of Divalent Thulium Borohydrides, and Their Application in  $\varepsilon$ -Caprolactone Polymerisation. *Chem. Commun.* **2011**, 47 (44), 12203–12205.
- (28) Hitchcock, P. B.; Lappert, M. F.; Maron, L.; Protchenko, A. V. Lanthanum Does Form Stable Molecular Compounds in the + 2 Oxidation State. *Angew. Chem., Int. Ed.* **2008**, 47 (8), 1488–1491.
- (29) Evans, W. J.; Allen, N. T.; Ziller, J. W. The Availability of Dysprosium Diiodide as a Powerful Reducing Agent in Organic Synthesis: Reactivity Studies and Structural Analysis of DyI2((DME)-3 and Its Naphthalene Reduction Product1. *J. Am. Chem. Soc.* **2000**, 122 (47), 11749–11750.
- (30) Bochkarev, M. N. Molecular Compounds of "New" Divalent Lanthanides. *Coord. Chem. Rev.* **2004**, 248 (9–10), 835–851.
- (31) Jaroschik, F.; Nief, F.; Le Goff, X.-F.; Ricard, L. Isolation of Stable Organodysprosium(II) Complexes by Chemical Reduction of Dysprosium(III) Precursors. *Organometallics* **2007**, *26* (5), 1123–1125
- (32) Jaroschik, F.; Nief, F.; Ricard, L. Synthesis of a New Stable, Neutral Organothulium(II) Complex by Reduction of a Thulium(III) Precursor. *Chem. Commun.* **2006**, No. 4, 426–428.
- (33) Cheng, J.; Takats, J.; Ferguson, M. J.; McDonald, R. Heteroleptic Tm(II) Complexes: One More Success for Trofimenko's Scorpionates. *J. Am. Chem. Soc.* **2008**, *130* (5), 1544–1545.
- (34) MacDonald, M. R.; Bates, J. E.; Ziller, J. W.; Furche, F.; Evans, W. J. Completing the Series of + 2 Ions for the Lanthanide Elements: Synthesis of Molecular Complexes of Pr2+, Gd2+, Tb2+, and Lu2+. *J. Am. Chem. Soc.* **2013**, 135 (26), 9857–9868.
- (35) Tricoire, M.; Hsueh, F.-C.; Keener, M.; Rajeshkumar, T.; Scopelliti, R.; Zivkovic, I.; Maron, L.; Mazzanti, M. Siloxide Tripodal Ligands as a Scaffold for Stabilizing Lanthanides in the + 4 Oxidation State. *Chem. Sci.* **2024**, *15*, 6874–6883.
- (36) Xue, T.; Ding, Y.-S.; Zheng, Z. A Tetravalent Praseodymium Complex with Field-Induced Slow Magnetic Relaxation. *Dalton Trans.* **2024**, *53* (13), *5779*–*5783*.
- (37) Tateyama, H.; Boggiano, A. C.; Liao, C.; Otte, K. S.; Li, X.; La Pierre, H. S. Tetravalent Cerium Alkyl and Benzyl Complexes. *J. Am. Chem. Soc.* **2024**, *146* (15), 10268–10273.
- (38) Flosbach, N. T.; Bykov, M.; Bykova, E.; Rasche, B.; Mezouar, M.; Fedotenko, T.; Chariton, S.; Prakapenka, V. B.; Wickleder, M. S. Stabilization of Pr4+ in Silicates-High-Pressure Synthesis of PrSi3O8 and Pr2Si7O18. *Inorg. Chem.* **2024**, *63* (11), 4875–4882.
- (39) Otte, K. S.; Niklas, J. E.; Studvick, C. M.; Boggiano, A. C.; Bacsa, J.; Popov, I. A.; La Pierre, H. S. Divergent Stabilities of Tetravalent Cerium, Uranium, and Neptunium Imidophosphorane Complexes\*\*. *Angew. Chem., Int. Ed.* **2023**, *62* (34), No. e202306580. (40) Willauer, A. R.; Douair, I.; Chauvin, A.-S.; Fadaei-Tirani, F.; Bünzli, J. C. G.; Maron, L.; Mazzanti, M. Structure, Reactivity and

- Luminescence Studies of Triphenylsiloxide Complexes of Tetravalent Lanthanides. *Chem. Sci.* **2022**, *13* (3), 681–691.
- (41) Fedushkin, I. L.; Yambulatov, D. S.; Skatova, A. A.; Baranov, E. V.; Demeshko, S.; Bogomyakov, A. S.; Ovcharenko, V. I.; Zueva, E. M. Ytterbium and Europium Complexes of Redox-Active Ligands: Searching for Redox Isomerism. *Inorg. Chem.* **2017**, *56* (16), 9825–9833
- (42) Fedushkin, I. L.; Maslova, O. V.; Morozov, A. G.; Dechert, S.; Demeshko, S.; Meyer, F. Genuine Redox Isomerism in a Rare-Earth-Metal Complex. *Angew. Chem., Int. Ed.* **2012**, *51* (42), 10584–10587.
- (43) Mrutu, A.; Barnes, C. L.; Bart, S. C.; Walensky, J. R. Bringing Redox Reactivity to a Redox Inactive Metal Center E-I (E = C, Si) Bond Cleavage with a Thorium Bis( $\alpha$ -Diimine) Complex. *Eur. J. Inorg. Chem.* **2013**, 2013 (22–23), 4050–4055.
- (44) Jori, N.; Toniolo, D.; Huynh, B. C.; Scopelliti, R.; Mazzanti, M. Carbon Dioxide Reduction by Lanthanide(III) Complexes Supported by Redox-Active Schiff Base Ligands. *Inorg. Chem. Front.* **2020**, 7 (19), 3598–3608.
- (45) Coughlin, E.; Bart, S. C. Reductive Silylation of Uranyl Mediated by Iminosemiquinone Ligands. *Polyhedron* **2019**, *170*, 783–787
- (46) Wang, D.; Tricoire, M.; Cemortan, V.; Moutet, J.; Nocton, G. Redox Activity of a Dissymmetric Ligand Bridging Divalent Ytter-Bium and Reactive Nickel Fragments. *Inorg. Chem. Front.* **2021**, 8 (3), 647–657.
- (47) Wang, D.; Moutet, J.; Tricoire, M.; Cordier, M.; Nocton, G. Reactive Heterobimetallic Complex Combining Divalent Ytterbium and Dimethyl Nickel Fragments. *Inorganics* **2019**, *7* (5), 58.
- (48) Huang, W.; Diaconescu, P. L. Reactivity and Properties of Metal Complexes Enabled by Flexible and Redox-Active Ligands with a Ferrocene Backbone. *Inorg. Chem.* **2016**, *55* (20), 10013–10023.
- (49) Brosmer, J. L.; Huang, W.; Diaconescu, P. L. Reduction of Diphenylacetylene Mediated by Rare-Earth Ferrocene Diamide Complexes. *Organometallics* **2017**, *36* (23), 4643–4648.
- (50) Dickie, C. M.; Laughlin, A. L.; Wofford, J. D.; Bhuvanesh, N. S.; Nippe, M. Transition Metal Redox Switches for Reversible "on/off" and "Slow/Fast" Single-Molecule Magnet Behaviour in Dysprosium and Erbium Bis-Diamidoferrocene Complexes. *Chem. Sci.* **2017**, 8 (12), 8039–8049.
- (51) Kynman, A. E.; Elghanayan, L. K.; Desnoyer, A. N.; Yang, Y.; Sévery, L.; Di Giuseppe, A.; Tilley, T. D.; Maron, L.; Arnold, P. L. Controlled Monodefluorination and Alkylation of C(Sp3)-F Bonds by Lanthanide Photocatalysts: Importance of Metal-Ligand Cooperativity. *Chem. Sci.* **2022**, *13* (47), 14090–14100.
- (52) Heyduk, A. F.; Zarkesh, R. A.; Nguyen, A. I. Designing Catalysts for Nitrene Transfer Using Early Transition Metals and Redox-Active Ligands. *Inorg. Chem.* **2011**, *50* (20), 9849–9863.
- (53) Munhá, Ř. F.; Zarkesh, R. A.; Heyduk, A. F. Tuning the Electronic and Steric Parameters of a Redox-Active Tris(Amido) Ligand. *Inorg. Chem.* **2013**, *52* (19), 11244–11255.
- (54) Belli, R. G.; Tafuri, V. C.; Joannou, M. V.; Roberts, C. C. D0Metal-Catalyzed Alkyl-Alkyl Cross-Coupling Enabled by a Redox-Active Ligand. *ACS Catal.* **2022**, *12* (5), 3094–3099.
- (55) Belli, R. G.; Tafuri, V. C.; Roberts, C. C. Improving Alkyl-Alkyl Cross-Coupling Catalysis with Early Transition Metals through Mechanistic Understanding and Metal Tuning. ACS Catal. 2022, 12 (15), 9430–9436.
- (56) Belli, R. G.; Tafuri, V. C.; Garcia, N. A.; Roberts, C. C. One-and Two-Electron Redox Catalysis with Lutetium Enabled by a Tris(Amido) Redox-Active Ligand. *Organometallics* **2023**, 42 (11), 1059–1064.
- (57) Gavin, J. T.; Belli, R. G.; Roberts, C. C. Radical-Polar Crossover Catalysis with a D0Metal Enabled by a Redox-Active Ligand. *J. Am. Chem. Soc.* **2022**, 144 (47), 21431–21436.
- (58) Wooles, A. J.; Mills, D. P.; Lewis, W.; Blake, A. J.; Liddle, S. T. Lanthanide Tri-Benzyl Complexes: Structural Variations and Useful Precursors to Phosphorus-Stabilised Lanthanide Carbenes. *Dalton Trans.* **2010**, 39 (2), 500–510.

- (59) Shannon, R. D. Revised Effective Ionic Radii and Systematic Studies of Interatomic Distances in Halides and Chalcogenides. *Acta Crystallogr., Sect. A* **1976**, 32 (5), 751–767.
- (60) Cordero, B.; Gómez, V.; Platero-Prats, A. E.; Revés, M.; Echeverría, J.; Cremades, E.; Barragán, F.; Alvarez, S. Covalent Radii Revisited. *Dalton Trans.* **2008**, No. 21, 2832–2838.
- (61) Pauling, L. Atomic Radii and Interatomic Distances in Metals. J. Am. Chem. Soc. 1947, 69 (3), 542–553.
- (62) Hoyer, E. Ionisation Constants of Inorganic Acids and Bases in Aqueous Solution: Zusammengestellt von D. D. Perrin; Oxford, New York, Toronto, Sidney, Paris, Frankfurt; Pergamon Press 1982; 2. Auflage, 180 Seiten; Pappb. \$ 50,00. Z. Chem. 1983, 23 (7), 276.
- (63) Moore, J. T.; Chatterjee, S.; Tarrago, M.; Clouston, L. J.; Sproules, S.; Bill, E.; Bernales, V.; Gagliardi, L.; Ye, S.; Lancaster, K. M.; Lu, C. C. Enhanced Fe-Centered Redox Flexibility in Fe-Ti Heterobimetallic Complexes. *Inorg. Chem.* 2019, 58 (9), 6199–6214.
- (64) Herrmann, W. A.; Denk, M.; Albach, R. W.; Behm, J.; Herdtweck, E. Cyclische Metall(IV)-Amide. *Chem. Ber.* **1991**, 124 (4), 683–689.
- (65) Willauer, A. R.; Palumbo, C. T.; Scopelliti, R.; Zivkovic, I.; Douair, I.; Maron, L.; Mazzanti, M. Stabilization of the Oxidation State + IV in Siloxide-Supported Terbium Compounds. *Angew. Chem., Int. Ed.* **2020**, *59* (9), 3549–3553.
- (66) Xue, T.; Ding, Y.-S.; Jiang, X.-L.; Tao, L.; Li, J.; Zheng, Z. Tetravalent Terbium Chelates: Stability Enhancement and Property Tuning. *Precis. Chem.* **2023**, *1* (10), 583–591.
- (67) Graves, C. R.; Scott, B. L.; Morris, D. E.; Kiplinger, J. L. Facile Access to Pentavalent Uranium Organometallics: One-Electron Oxidation of Uranium(IV) Imido Complexes with Copper(I) Salts. J. Am. Chem. Soc. 2007, 129 (39), 11914–11915.
- (68) Gompa, T. P.; Greer, S. M.; Rice, N. T.; Jiang, N.; Telser, J.; Ozarowski, A.; Stein, B. W.; La Pierre, H. S. High-Frequency and -Field Electron Paramagnetic Resonance Spectroscopic Analysis of Metal-Ligand Covalency in a 4f7 Valence Series (Eu2+, Gd3+, and Tb4+). *Inorg. Chem.* **2021**, *60* (12), 9064–9073.
- (69) Ishii, M.; Morihashi, K.; Kikuchi, O. Calculation of G-Values of Free Radicals by Finite Perturbation Theory. *J. Mol. Struct.: THEOCHEM* **1989**, *187*, 209–218.
- (70) Pritchard, B. P.; Altarawy, D.; Didier, B.; Gibson, T. D.; Windus, T. L. New Basis Set Exchange: An Open, Up-to-Date Resource for the Molecular Sciences Community. *J. Chem. Inf. Model.* **2019**, *59* (11), 4814–4820.
- (71) van der Vlugt, J. I. Radical-Type Reactivity and Catalysis by Single-Electron Transfer to or from Redox-Active Ligands. *Chem. Eur. J.* **2019**, 25 (11), 2651–2662.
- (72) Singh, K.; Kundu, A.; Adhikari, D. Ligand-Based Redox: Catalytic Applications and Mechanistic Aspects. *ACS Catal.* **2022**, *12* (20), 13075–13107.